River Bathymetry Extraction Using High-Resolution Aerial Digital Imagery

Maxim Bulat

GEOG 491 – Honours Thesis Seminar

Completed 2015

Abstract

River bathymetry is a key variable in hydrological studies. Since it is important to characterize rivers as holistic systems at the scale of the whole watershed, traditional methods of data collection are not suitable as they are labour intensive and time consuming. Fluvial remote sensing could become a potential solution to the problem by providing methods of riverine feature extraction, including riverbed topography. Recent advances in technology allow the use of unmanned aerial vehicles (UAV), which are less expensive and offer higher spatial resolution than data acquired from helicopter, airplanes or satellites. Remote sensing conventionally measure either multi-spectral or hyper-spectral data, comprising of many narrow spectral bands and is less available than the true-colour imagery. There are, however, few studies in fluvial remote sensing that address the use of widely available digital cameras to obtain true-colour (RGB) photos. This study will aim to address the gap in the literature by (1) attempting to predict bathymetry from true-colour images in a river reach using the correlational, hydraulically assisted bathymetry (HAB-2) and band ratio algorithms; and (2) assessing the accuracy of depth prediction and applicability of the aforementioned models in environments different from where these models were developed. Results show that the overall performance of all approaches was poor with unsatisfactory results based on R^2 and Nash-Sutcliffe Efficiency Model coefficients. Nonetheless, the correlational and HAB-2 models showed limited minimal applicability to historical data, or to relative depth mapping.

Acknowledgements

The completion of this research would not have been possible without the supervision and support of Dr. Pascale Biron and Dr. James Freeman. I am also very grateful for the funding provided by NSERC, which allowed me to conduct research during the summer of 2014. The UAV provided by the Geography Undergrad Student Society Concordia was vital in this study. A special thank you to William Massey for assisting in the field data collection, Guénolé Choné for providing river slope data for the study reach and his insight into the statistical data analysis as well as Fabien Hugues for his willingness to share his views on bathymetry prediction.

Table of Contents

1. Introduction 1

2. Literature Review 5

2.1 Bathymetry extraction 5

2.1.1 Bathymetry prediction and conventional in-river measurements 5

2.1.2 Role of UAV in remote sensing 7

2.1.3 Data sources 8

2.1.4 Challenges reported 9

2.1.5 Approaches to Bathymetry Extraction 11

2.2 Research Objectives 12

3. Methodology 14

3.1 Field site 14

3.2 Depth measurements 15

3.3 UAV imagery 17

3.4 Geomont orthorectified photos 20

4. Post-processing 22

4.1 Georeferencing datasets 22

4.2 River body extraction 22

4.3 Correlational model 23

4.4 HAB–2 Model 24

4.5 Band Ratio Model 27

5. Results 28

6. Discussion 35

7. Conclusion 40

References: 43

Table of Figures:

Figure 1: Location of the study river reach 14

Figure 2: Portion of the Yamaska Sud-Est River used as the study reach 15

Figure 3: The marker used to overlay the UAV images and the field topography data. 16

Figure 4: The UAV original corrected images (left) and the extracted red band (right) with the overlaid field surveyed topography points 17

Figure 5: The UAV provided by GUSS and used for data collection 18

Figure 6: The programmed GPS points for the autonomous UAV flight over the study river reach in the Mission Planner 19

Figure 7: The programmed flight mission in the Mission Planner 19

Figure 8: The unedited and exposure corrected original UAV photo 20

Figure 9: The resulting bathymetry maps produced by the correlation of the red band (A), HAB-2 (B) and the band ratio (C) models. 29

Figure 10: The relative comparison of the bathymetry maps produced by HAB-2 model for the UAV (A) and Geomont data (B) 30

Figure 11: Correlation of predicted and measured depths for the correlational (A), HAB-2 (B) and band ratio (C) models 32

Figure 12: The outliers resulting from shadows 33

Figure 13: Correlation of predicted and measured depths per zone for the correlational (A), HAB-2 (B) and band ratio (C) models. 34

Figure 14: The depth overestimation resulting from the presence of shadows 37

Table list:

Table 1: Coefficient values resulting from the linear regression of the predicted and observed depths 28

Table 2: The equations derived from the algorithm calibrations 28

Table 3: Correlation and NSE coefficients for the predicted and measured depths per zone 33

1. Introduction

Remotely sensed (RS) information is increasingly part of our daily life, for example to provide data used in weather forecasting, land feature mapping, time change detection of various environmental phenomena and many other scientific applications (Carbonneau and Piégay, 2012). Remotely acquired imagery is a particularly valuable tool in studies of forestry (Dunford et al., 2009), geology (Metternicht et al., 2005), agriculture (McKenzie and Ryan, 1999), biology and hydrology (Wirth et al., 2012; Whited et al., 2013). With the introduction of many remote–sensing platforms such as satellites, helicopters, planes or unmanned aerial vehicles (UAV), landscape feature extraction has become even more accessible.

Although the remote sensing technologies and instruments have been available since the 1970's, when NASA started its Landsat satellite program, the development paths of the remote sensing and fluvial studies did not truly cross until the last decade. Commonly in the field of remote sensing, rivers were extracted in two dimensions either as linear features depending on the scale, or a network of connected lines and lakes (Carbonneau and Piégay, 2012). Due to the fact that rivers are highly dynamic on the temporal scale (Whited et al., 2002), the necessity of frequently surveying and monitoring rivers is a key component of many hydrological studies and requires on the knowledge of the three-dimensional geometry (Feurer et al., 2008). Fluvial scientists such as geomorphologists, riparian and lotic ecologists pay much attention to the internal structures and processes that govern rivers, and represent them spatially in three dimensions, but from a highly localized aspect. These viewpoints need to be reconciled, as pointed out by

Carbonneau and Piégay (2012), since neither of these views considers the fact that many biotic and abiotic processes in nature operate on larger spatial scales than those covered conventionally by present river studies (Fausch et al., 2002).

Fonstad and Marcus (2010) argue that most of river research methods are not suitable for both watershed-extent and local characterization and data collection, since in both cases the data is collected in smaller areas (either several places throughout the river catchment, or a single place in the river). Rivers are very productive geomorphological environments, supporting high riverine biodiversity such as pools, riffles, glides and runs (Whited et al., 2013). Up until now, the river morphology and habitats have been sampled either by high resolution localized points or surveyed over a broader spaced extents, through cross-section measurements and extrapolation (Winterbottom and Gilvear, 1997), providing average trends throughout a watershed (Carbonneau et al., 2012) and representing river habitats as nothing else than a coarse approximation (Flener et al., 2013).

Exploring rivers in smaller reaches creates a "fundamental scale mismatch between the occurring processes and data collection" (Carbonneau and Piégay, 2012, p. 1). Fausch et al. (2002), as cited by Carbonneau and Piégay (2012), argue that the rivers need to be considered and sampled as holistic systems and larger spatial units, covering entire watersheds. A similar opinion expressed by Whited et al. (2002) states that rivers play a vital role in large ecosystems, and it is important to characterize them on larger extents than what was done in the past.

Following the given recommendations on sampling rivers as holistic systems and river catchments, it is evident that remote sensing is becoming a methodology

of choice. It is the only feasible approach that allows collection of continuous data over the whole catchment area. In the 1990s and early 2000s the existing remote sensing instruments and analytical methods, as well as the spatial resolution, were not really appropriate for the needs of fluvial science (Carbonneau et al., 2012). The riverine features extracted from the remotely sensed data were mostly on hectametric or kilometric scales (Carbonneau et al., 2012). However, the rapid technological development in the field of remote sensing in the last decade permitted data capturing at finer resolutions, allowing extracting riverine features on microhabitat level. Advances in remote sensing were followed by an increasing number of published papers on fluvial remote sensing (FRS), highlighting the onset of a new sub-discipline (Carbonneau et al., 2012).

Conventionally remote sensing can be achieved by using either passive, measuring the reflected solar energy, or active sensors, recording the return of the emitted pulses of energy by instruments (Carbonneau and Piégay, 2012). In this study, only optical imagery is being taken into consideration and it includes the part of the spectrum visible to the human eye that is the blue, green, and red bands. The three bands as well as the near-infrared and infrared are the dominant wavelengths coming from the Sun electromagnetic energy (Carbonneau and Piégay, 2012). The other types of available active technologies, such as radar or LiDAR are not considered in this study. It should be noted as well that all the methods, which are examined and discussed in this study consider only the active submerged river channel, which experiences erosion and deposition due to typical hydrological conditions.

The thesis would discuss the body of literature that specifically focuses on the fluvial remote sensing, the riverbed depth estimation and the gaps, which are not covered by other relevant studies. A short introduction to approaches suggested for examination will be covered in the literature review. The study river reach, data sources and methodology would be presented and explained, followed by reporting of the obtained results and their discussion. Finally a conclusion will be drawn based on the findings, including suggestions for improvement.

2. Literature Review

2.1 Bathymetry extraction

2.1.1 Bathymetry prediction and conventional in-river measurements

Recent fluvial remote sensing studies have revealed that key habitat information such as median surface gravel size (Carbonneau et al., 2004), bed topography (Fonstad and Marcus, 2005; Carbonneau et al., 2006; Flener et al., 2012; Legleiter, 2013), woody debris (Dunford et al., 2009), substrate type (Gilvear et al., 2007), submerged aquatic vegetation (Visser et al., 2013) can be obtained from airborne imagery with the use of algorithms developed by researchers. Furthermore, flood extents and discharge can be derived on a regular basis and may be used as an early warning in areas without hydrological monitoring systems (Carbonneau and Piégay, 2012). Temporal channel change, in terms of mapping channel boundaries, bars, floodplain cover, erosion, is yet another application for fluvial remote sensing (Gilvear and Bryant, 2003) as well as turbidity, suspended sand bed sediment, biotypes otherwise known as in-stream habitat or morphological units (Carbonneau and Piégay, 2012).

It is worth mentioning other potential directions for remote sensing applications in fluvial studies such as forecasting and detection of ice breakup on large sub-polar and polar rivers, and use of remotely sensed derived stream variables in stream power estimation, though it requires both passive and active sensors (Carbonneau and Piégay, 2012).

Comprehensive information on river bathymetry (channel topography) is key to characterize stream hydraulics (Waddle et al., 2000), model flow dynamics and

forecast flood hazards (Lane and Chandler, 2003), as well as in predicting channel change (Lane et al., 2002) and monitoring, mapping and modeling in-stream habitats (Whited et al., 2002; Marcus et al., 2003; Carbonneau and Piégay, 2012). Airborne true-colour imagery can be used for channel depth mapping, even when the field-surveyed measurements are not available or not taken (Carbonneau et al., 2012).

The need for describing riverbed topography throughout the whole catchment area has been discussed by many authors as there is a clear consensus that the previous methods of depth mapping did not offer continuity of the observed depth data along rivers, which is imperative in river studies (Hilldale and Daff, 2008; Fonstad and Marcus, 2010; Kinzel et al., 2012; Flener, 2013). Conventional field data collection of the riverbed topography is labour intensive (Legleiter, 2003; Marcus et al., 2003; Walther et al., 2012), time and resource consuming (Winterbottom and Gilvear, 1997; Legleiter and Overstreet, 2012; Moretto et al., 2014) and thus is not practical on a large scale. Often the information on bathymetry from the past is unavailable or rivers are inaccessible in certain areas for field data collection (Winterbottom and Gilvear, 1997; Feurer et al., 2008).

The conventional methods of depth measurement offer high-resolution and precise data, the level of which cannot be achieved by current depth prediction algorithms (Fonstad and Marcus, 2005; Carbonneau et al., 2006; Gilvear et al., 2007; Legleiter et al., 2009). Nonetheless, considering the extrapolation required to ground-based point data and the extents to which remote sensing could be applied, the depth prediction from airborne data sets still offers a great potential

(Winterbottom and Gilvear, 1997; Whited et al., 2002) to create coherent hydraulically correct depth maps (Westaway et al., 2001; Legleiter, 2012,). This can be achieved by combining different data sources to create digital elevation models (DEM) for both riverbed topography and riparian zone, for example by combining active RS and optical passive RS (Westaway, 2001; Hilldale and Raff, 2008; Legleiter, 2012).

2.1.2 Role of UAV in remote sensing

UAVs are becoming increasingly available to the public. Some of them offer basic functionality, whereas others are more sophisticated, robust and are bundled with specialized software, which allows seamless sieving of the captured images and generation of digital elevation models (DEM). Overall, UAV provide low cost, high efficiency and quick deployment data with operational flexibility, high vertical accuracy, and centimeter-scale resolution (Tamminga et al., 2014). UAVs thus present a possibility of acquiring data in a fast and accurate way when multi–temporal data are required (Flener et al. ,2013). There are, however, some limitations related to the width of the river channel (several flights may be required for wide channels), weather conditions (wind speeds should be less than 5-10 m/s) and presence of clouds between different flights (Flener et al, 2013).

The size of UAV determines the legal responsibility, since this sector is relatively new and the legislation has not yet been "polished" enough to cater for different uses and UAV types. In fluvial remote sensing mini-UAVs are mostly used with installed inexpensive point–and–shoot digital cameras. Under current

legislation restrictions, the maximum weight allowed for take off is 20-25 kg, the unit has to remain in line–of–sight and flown at an altitude below 150 m or 400 feet (Flener et al., 2013). The introduction of the 'line–of–sight' restriction limits the distance of UAV flights and thus smaller area could be covered per flight. Other aforementioned restrictions affect less UAVs, which are typically used in fluvial remotes sensing, since the cameras are relatively light and rarely exceed 500 g on average, 1 kg being an extreme weight and relates more to digital single–lens reflex cameras (DSLR). The altitude of less than 150 m offers higher spatial resolution achieved in the taken digital images. In addition, no atmospheric interference would be observed and thus it would not require any corrections.

2.1.3 Data sources

Most of the studies report successful results while using the optical passive sensors, which are capable of producing multi- and hyperspectral images coming either from satellites such as IKONOS (Marcus and Fonstad, 2008), WorldView2 (Legleiter and Overstreet, 2012), or airborne platforms (Legleiter, 2003; Marcus et al., 2003; Legleiter and Roberts, 2005). Some of the authors agree that the near-infrared band, despite being very sensitive to the water depth due to its absorption by water, is limited to the maximum depth and is not useable for deep rivers (Legleiter et al., 2004). Legleiter et al. (2009) have developed optimal band ratio analysis (OBRA) tool, which assists in finding the best suitable bands from available multispectral imagery, the ratio of which would provide the best estimate of the depth.

A few scholars researched the feasibility of using data sets excluding the near-infrared band, coming either from printed archival imagery, covering the past decades or digital true-colour images (Lane et al., 2010). Though the riverbed topography could have been predicted in these studies, certain issues have been reported (Fonstad and Marcus, 2005; Carbonneau et al., 2006; Flener et al., 2012). The printed images, originally coming as black and white photos, must be scanned thus introducing image noise and added accuracy errors in both geometry and colour rendering (Walther et al., 2012).

There are a few studies that have attempted to apply the airborne LiDAR Bathymetry (ALB) to depth prediction (Hilldale and Raff, 2008; Kinzel et al., 2012). Both Hilldale and Raff (2008) and Kinzel et al. (2012) specify that the bathymetric LiDAR overcomes some of the limitations met while deploying optical passive surveying, though limited ALB availability and lack of microscale precision prevents it from being widely used at the moment (Hilldale and Raff, 2008). Moreover, the system might not be applicable yet due to some hardware limitations and safety concerns (Kinzel et al., 2012).

2.1.4 Challenges reported

Although the airborne data collection seems to be straightforward with a RS system flying over study area(s), several challenges remain.

Within the acquisition time period (it could be several days if longer reaches have to be covered) the illumination levels could change, thus bringing some variation from one image to another, and requiring some correction to be applied so

that the model results would not differ between images (Carbonneau et al.,2006). Water turbidity is also a major issue when trying to extract bed topography, resulting in false bed bottom problems (Fonstad and Marcus, 2005; Carbonneau et al., 2006; Feurer et al., 2008; Marcus and Fonstad, 2008; Legleiter and Roberts, 2009; Flener et al., 2012) This results mainly from the suspended sediment back scattering problem (Kinzel et al., 2012).

Other reported problems in the literature pertain to water surface turbulence, which severely limits the accuracy of depth predictions, since the water becomes opaque and the riverbed may not be visible (Legleiter et al., 2004; Marcus and Fonstad, 2010). Sun glint and shadows on water surface are another source of concern (Roberts and Anderson, 1999; Feurer et al., 2008; Flener et al., 2012;). In this regard airborne studies should ideally be carried out between 11.00 AM and 1.00 PM, to eliminate shadows as much as possible.

Another issue reported by many authors is the presence of the overhanging bank vegetation, which hides parts of river channel from the airborne optical systems (Legleiter and Roberts, 2005; Carbonneau et al., 2006; Flener et al., 2012). Bank vegetation contributes as well to the presence of water surface shadows, which overestimate the depths in certain river segments (Fonstad and Marcus, 2005; Flener et al., 2012; Legleiter and Overstreet, 2012). Thus, other algorithms must be developed to eliminate these obstacles. Bird et al. (2010) propose another approach and a possible solution, where digital camera is being transported under the riparian canopy over a stream. It is reasoned that this approach could be applied

to smaller streams (Bird et al., 2010), since the camera is being transported by a 10-meter unipod. It is not clear if this approach would be applicable to wider rivers.

The aforementioned challenges such as shadows and lighting limitations could be eliminated by using ALB as it has been shown by Hilldale and Raff (2008), Kinzel et al. (2012), though the accessibility of ALB systems is currently limited.

2.1.5 Approaches to Bathymetry Extraction

Several approaches have been proposed to obtain depth predictions (Gilvear et al. 2007; Hilldale and Daff, 2008; Marcus and Fonstad, 2008; Legleiter et al. 2009; Carbonneau and Piégay, 2010; Legleiter, 2013). Most of these approaches require two data sets to be collected – remotely sensed and ground surveyed, although Fonstad and Marcus (2005), Lane et al. (2010), Walther et al. (2012) and Legleiter (2013) argue that it is possible to derive the river bathymetry from aerial imagery without the need of collecting ground-truth data. Thus it could be possible to obtain depth from archived imagery and therefore to detect changes over a longer period of time. Fonstad and Marcus (2005) and Walther et al. (2012) proposed hydraulically assisted bathymetry (HAB) models, applicable to the red band, which is the most sensitive to depth variation. While this approach offers consistent results, other scholars argue that by using only one band out of three, the differences in substrate colour and types are not considered (Carbonneau and Piégay, 2012). An improvement to this approach has been suggested by Legleiter and Roberts (2005), which consists in using the green to red band ratio, thereby

eliminating differences between the substrate type and colour (Legleiter and Roberts, 2005; Legleiter et al., 2009).

Flener et al. (2012) tested HAB models outside of the environment where these models have been developed and tested, arguing that some of the parameters used in HAB models are rather sensitive, such as the channel friction parameter. At the same time Flener et al. (2012) compared the results of an empirical approach based on Lyzenga's (1981) method. Lyzenga's algorithm was developed to obtain the information on river bottom information, where the bottom-reflected radiance is a linear function of bottom reflectance and an exponential function of water depth (Lyzenga, 1981). Although initially the algorithm has been suggested specifically to obtain the data on the marine substrate type from multispectral imagery, other researchers applied it to river depth extraction (Winterbottom and Gilvear, 1997). Under certain conditions, HAB models may approach the accuracy of Lyzenga's algorithm but otherwise would produce relatively correct depth maps but with less accuracy (Flener et al., 2012). The Lyzenga's method requires the water reflectance measurement from areas deeper than the light could penetrate (Flener et al., 2012), which may not always be possible in shallow water environments such as in the study of Winterbottom and Gilvear (1997).

2.2 Research Objectives

There is a clear consensus in the literature that river bathymetry can be extracted from airborne high-resolution multi- and hyper-spectral imagery. Algorithms such as HAB models, Lyzenga method, correlational approaches and

band rationing all have the potential to be developed and become a trustworthy and reliable tool in riverbed topography quantification. Fewer studies have attempted to assess the usefulness of airborne true-colour RGB images, excluding the near-infrared band in depth extraction.

The research questions this study will aim at answering are:

1) Could high-resolution true-colour imagery be used for bathymetry prediction?

2) Are the suggested algorithms applicable outside the areas where they have been developed with consistent results when compared to field surveys?

These research questions will be addressed using a case study in a gravel-bed reach of the Yamaska Sud-Est River (Qc).

With the increasing availability of true-colour imagery through the use of drones, results will provide a key insight on the feasibility of using RGB images in bathymetry prediction in large-scale studies for shallow sand and gravel-bed rivers, and whether such riverbed topography maps may be used in further studies requiring depth information.

3. Methodology

3.1 Field site

A study reach of approximately 200 m in length in the Yamaska Sud-Est River (near Cowansville, Qc, Figure 1) was used for field surveying and 400 m for remote sensing was chosen for this project based on the following considerations:

1) Low water turbidity;
2) Relatively shallow and wadeable reach for safe field surveying, with maximum depths of 1.4 m;
3) Width of the channel sufficiently big not to be covered by overhanging vegetation (10–30 m wide).
4) Open area nearby in order to fly the UAV in autonomous mode (250x250 m^2 for automatic landing purposes as recommended by the operational instructions)
5) Accessibility (close to a road) to carry the equipment.

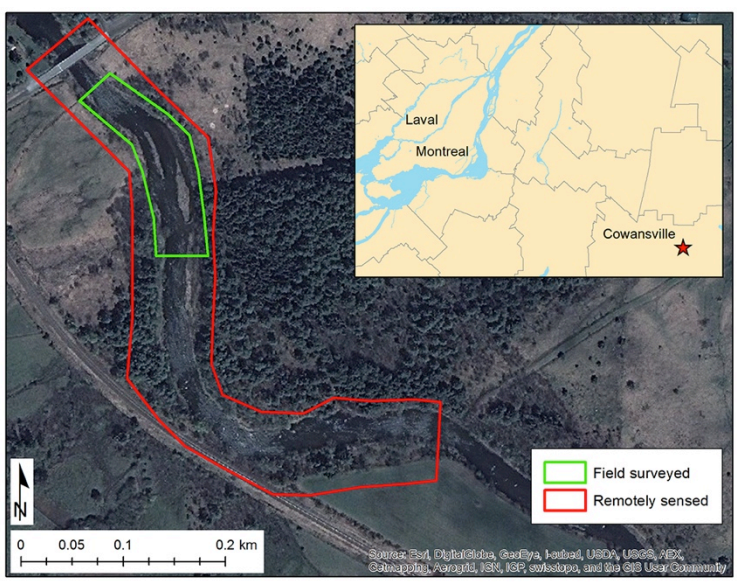

Figure 1: Location of the study river reach.

At the time of data collection the Yamaska Sud-Est River was at low flow stage with discharge estimated at the gaging station #030314 averaging 2.659 m^3/s for August 16, 2014. The average depth of the submerged channel was 36 cm. The channel width ranged between 21 m and 36 m in the study reach. The slope of the study reach is 0.0017 (Choné, 2013). A riffle (shallow, fast zone) and a pool (deeper, slower zone) were located within the study reach. The substrate consisted of elongated patches of sand and gravel in the shallowest section, large boulders randomly found through the reach (see Figure 2) as well as cobbles in the riffle section.

Figure 2: Portion of the Yamaska Sud-Est River used as the study reach (looking upstream)

3.2 Depth measurements

The 200-m study reach was surveyed on August 16, 2014, between 12.00 and 3.00 PM, to provide data for the calibration of the correlational and band ratio models, and validation of the accuracy of depth prediction resulting from the correlational, HAB-2 and band ratio models. The depth measurements have been

taken with a Leica TC805L Total Station (accuracy of ±1 cm) and required a team of two people. Immediately following the flight of the UAV, which belongs to Concordia Geography Undergrad Student Society (GUSS), 290 points were surveyed, including the height of water surface and marker (see Figure 3) positions on the banks and the bar located in the middle of the reach. 210 points out of 290 contained the depth information. The entire reach was covered by five cross-sections, numbered 1 to 5 from downstream to upstream. Additional depth measurements were taken in-between cross-sections to supplement and represent the river topography both planimetrically and vertically (Figure 4). At points located between cross-sections, the water surface height was also recorded to obtain more accurate field depth estimations.

The surveying unit records the (X, Y, Z) coordinates of each point. These data were imported into Microsoft Excel to compute the actual depth measurements (difference between water surface and bed measurements). The average water surface height has been calculated for cross-section 3, since there was a discrepancy of up to 2 cm between the banks and the bar, and used for depth calculation along the cross-section.

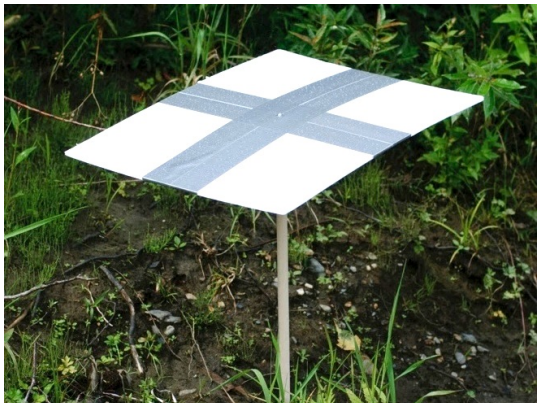

Figure 3: The marker used to overlay the UAV images and the field topography data.

The positions of five markers were used for georeferencing the dataset to an absolute datum and to overlay the surveyed points with the imagery obtained from the UAV camera.

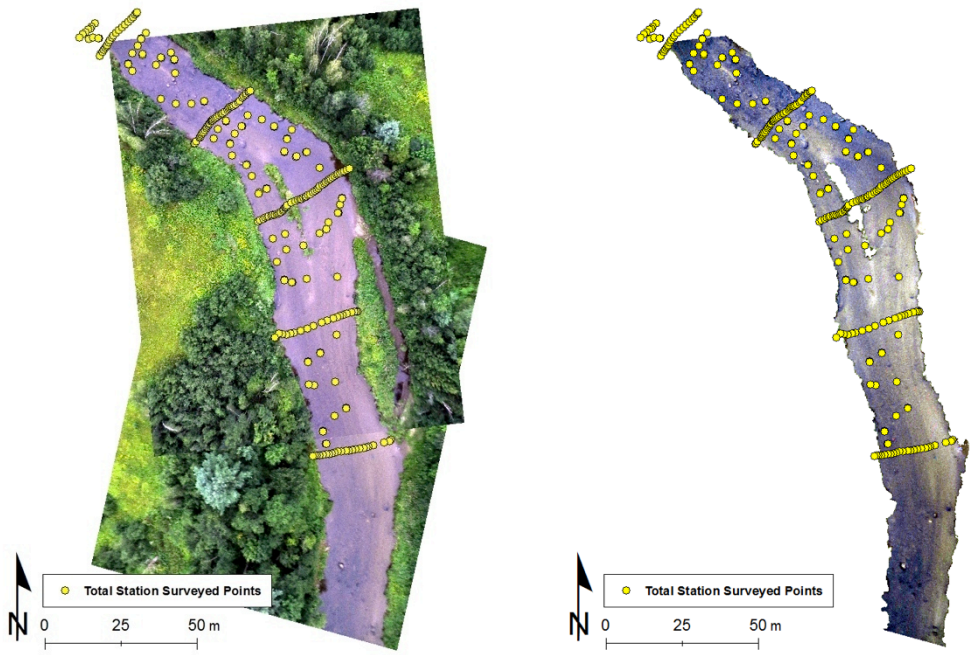

Figure 4: The UAV original corrected images (left) and the extracted red band (right) with the overlaid field surveyed topography points.

3.3 UAV imagery

The UAV dataset was acquired on August 16, 2014, prior to the field survey between 11.20 – 11.30 AM. The Canon PowerShot SX260HS camera installed on board of Skywalker UAV platform (see Figure 5) captured a sequence of images during its flight. Two photos out of this sequence were selected to be used in this study, as they covered completely the surveyed reach. The camera had third party firmware installed, which allowed the use of timer scripts for autonomous in-flight

photo taking. The UAV was pre-programmed with a flight mission, which had been loaded into the autopilot APM 2.6 module ('APM 2.6 Set - 3DRobotics Inc', n.d.).

Figure 5: The UAV provided by GUSS and used for data collection.

The mission consisted of pre-set GPS points (global positioning system coordinates), which followed the river channel, and take-off and landing positions, which permitted to fly it autonomously at an altitude of 100 m above the river surface. The UAV came with uBlox GPS module ('3DR uBlox GPS with Compass Kit - 3DRobotics Inc', n.d.) attached to the UAV autopilot, which made it possible to follow the flight mission. It was programmed (see Figures 6 and 7) in the Mission Planner software ('Mission Planner | Ground Station', n.d.), which is freely distributed and has no usage restrictions. The purpose of flying the UAV in autonomous mode was to test the feasibility of using relatively inexpensive remotely controlled plane model for fluvial remote sensing, its capability to carry out autonomous flights as well as autonomous take-offs and landings.

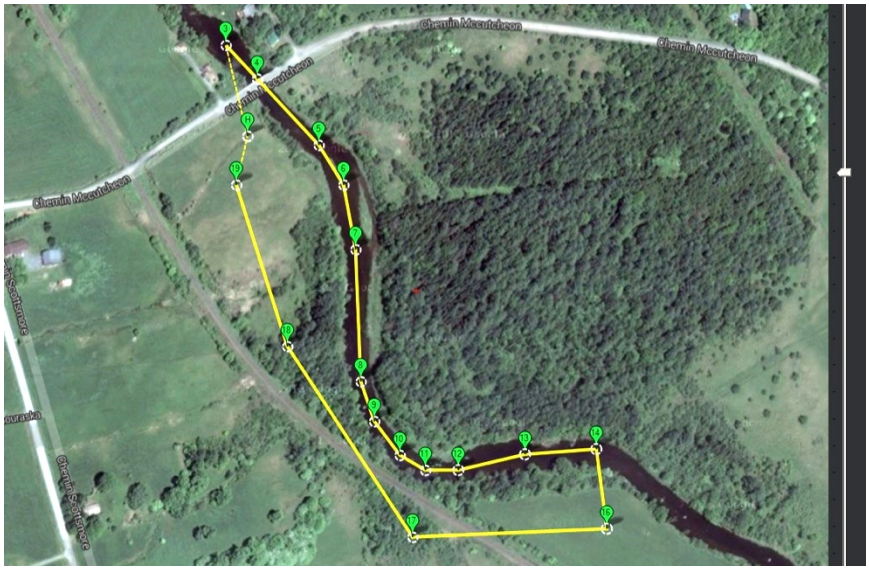

Figure 6: The programmed GPS points for the autonomous UAV flight over the study river reach in the Mission Planner.

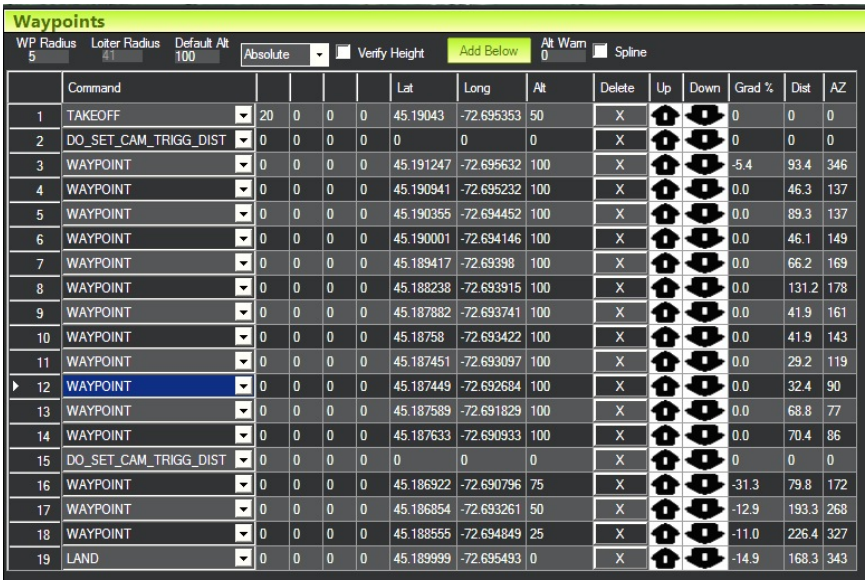

Waypoints

WP Radius 5 | Loiter Radius 41 | Default Alt 100 | Absolute | Verify Height | Add Below | Alt Warn 0 | Spline

	Command					Lat	Long	Alt	Delete	Up	Down	Grad %	Dist	AZ
1	TAKEOFF	20	0	0	0	45.19043	-72.695353	50	X			0	0	0
2	DO_SET_CAM_TRIGG_DIST	0	0	0	0	0	0	0	X			0	0	0
3	WAYPOINT	0	0	0	0	45.191247	-72.695632	100	X			-5.4	93.4	346
4	WAYPOINT	0	0	0	0	45.190941	-72.695232	100	X			0.0	46.3	137
5	WAYPOINT	0	0	0	0	45.190355	-72.694452	100	X			0.0	89.3	137
6	WAYPOINT	0	0	0	0	45.190001	-72.694146	100	X			0.0	46.1	149
7	WAYPOINT	0	0	0	0	45.189417	-72.69398	100	X			0.0	66.2	169
8	WAYPOINT	0	0	0	0	45.188238	-72.693915	100	X			0.0	131.2	178
9	WAYPOINT	0	0	0	0	45.187882	-72.693741	100	X			0.0	41.9	161
10	WAYPOINT	0	0	0	0	45.18758	-72.693422	100	X			0.0	41.9	143
11	WAYPOINT	0	0	0	0	45.187451	-72.693097	100	X			0.0	29.2	119
12	WAYPOINT	0	0	0	0	45.187449	-72.692684	100	X			0.0	32.4	90
13	WAYPOINT	0	0	0	0	45.187589	-72.691829	100	X			0.0	68.8	77
14	WAYPOINT	0	0	0	0	45.187633	-72.690933	100	X			0.0	70.4	86
15	DO_SET_CAM_TRIGG_DIST	0	0	0	0	0	0	0	X			0	0	0
16	WAYPOINT	0	0	0	0	45.186922	-72.690796	75	X			-31.3	79.8	172
17	WAYPOINT	0	0	0	0	45.186854	-72.693261	50	X			-12.9	193.3	268
18	WAYPOINT	0	0	0	0	45.188555	-72.694849	25	X			-11.0	226.4	327
19	LAND	0	0	0	0	45.189999	-72.695493	0	X			-14.9	168.3	343

Figure 7: The programmed flight mission in the Mission Planner.

The selected images represent typical RGB JPEG digital photos. The sky was heavily overcast during the UAV flight, and the selected capturing parameters such as aperture of f/3.5 and shutter speed of 1/800 s at 200 ISO speed caused underexposure (see Figure 8) in images, which were later corrected for exposure (see below). No other corrections, such as white balance, brightness-contrast, or

vignette removal, etc., have been applied to the images. Due to lower flying altitude and high camera resolution, it was possible to achieve ~4 cm/pixel spatial resolution. The dimensions of images are 4000x3000 pixels, representing 19,200 m^2 of terrain per photo. All images overlap each other by approximately 50%.

Figure 8: The unedited original UAV photo (left) and the same photo corrected for exposure (right).

3.4 Geomont orthorectified photos

To test HAB-2 model for its applicability to historical images, where no field depth measurements are available, photos produced and distributed by Geomont (http://www.geomont.qc.ca/orthophoto-20140/) were used in this study. The photos were taken on May 7, 2014 at 2.22 PM. The average discharge for that day was estimated to be 7.047 m^3/s. These are RGB JP2 images offering coarser 30 cm/pixel spatial resolution, which is yet acceptable for riverbed depth prediction (Carbonneau and Piégay, 2012). The images were originally georeferenced and

geometrically corrected by Geomont, and no other corrections were required prior to HAB-2 model calibration. The orthorectified photos are distributed as original files containing the near-infrared band, as well as processed true-colour composite images having only the blue, green and red bands. In this study only the true-colour photos have been tested, as the available archival aerial photo sets are stored as prints or films, requiring to be scanned, or as RGB digital images, thus no infra-red band is available. The images belonging to this dataset were taken under different flying conditions than the UAV, such as higher altitude and different capturing platform. The images also represent spatially larger terrain area on a single photo. The dimensions of a photo produced by Geomont are 10,894x11,355 pixels, representing 37,110,411 m^2 or ~37 km^2. To cover the selected study river reach, only single image was required.

4. Post-processing

4.1 Georeferencing datasets

The photos obtained from the UAV camera were downloaded to a computer and corrected for the underexposure in Adobe Photoshop software. The two images covering the reach area were imported into ArcGIS software and converted into GeoTIFF files, using the georeferencing toolbar, with a reported error of 14 cm. Due to considerable tilt of the camera at the moment of the first image capture, cross-section 1 was not represented geometrically correct and was excluded from model calibration and validation. Once the aerial photos from the UAV dataset were positioned, the total station data were overlaid on them by linking the marker positions on both the photos and the surveyed data using the Spatial Adjustment toolbar in ArcGIS software with 13 cm error in accuracy. The surveyed topography points correctly overlaid the river channel and were used later as points for pixel value extractions for all the models. The orthorectified photos supplied by Geomont were already georeferenced to an absolute datum and did not require additional geo-referencing.

4.2 River body extraction

To test the different depth extraction models, the river channel first needed to be extracted from the available images (UAV image set and Geomont orthophotos). This was achieved in Exelis ENVI software, using the Band Math tool. The principle of the Normalised Water Difference Index (NDWI) was used in the procedure, where a ratio using the blue and red bands, such as

$$(NDWI = \frac{(Blue\ Band - Red\ Band)}{(Blue\ Band + Red\ Band)}) \qquad 1)$$

would produce an image with floating point values ranging from –1.0 to 1.0. The threshold cut-off of 0.65 was then applied to differentiate the river from the rest of the images and create mask layers. These mask layers were used in the supervised classification in the <Classification Workflow> in Exelis ENVI software, and the river channel shapefile was generated. The shapefile were imported into ArcGIS software together with the images from the UAV and Geomont datasets. Since the vector shape did not follow exactly the channel borders and included either some parts of banks or exposed boulders in the river, some manual vector editing in ArcGIS was required. Following this step the river channel was clipped, removing all pixels irrelevant to the river channel (representing banks, vegetation, and some human-built infrastructure, like the nearby bridge and the road). Once the river channel was separated from the rest of the images, the green and red bands were extracted as separate GeoTIFF files for further data manipulation. They were smoothed with low pass filter.

4.3 Correlational model

The pixel values extracted from the red band were compared with the field measurements to obtain a correlation value. The pixel values were extracted in ESRI ArcGIS with <Extract Values To Points> tool and were attached to the attribute table of the shapefile, representing the surveyed topography points. The table was then exported to Microsoft Excel for further processing. The Excel table was then imported into R software for statistical analysis such as regression analysis. The

obtained equation, which represented the best-fit line from the linear regression of the red band pixel values and the observed field measurements, was applied to the original band raster in ArcGIS software with the <Raster Calculator> tool. This resulted in a bathymetry map, which provided the predicted depths in the study river reach.

To assess the accuracy of the prediction done by the approaches, similar steps to the aforementioned procedure were performed. The pixel values from the newly created depth map were extracted to the original topography shapefile, having the field depth measurements and using the same <Extract Values To Points> tool. The attribute table from the shapefile was exported as database file and processed in Microsoft Excel to include this time only the predicted and the observed depths.

The Nash-Sutcliffe model efficiency coefficient (NSE) was calculated at this step to assist with the comparison of the three approaches. The coefficient is calculated using the following formula:

$$NSE = 1 - \frac{\Sigma(P-O)^2}{\Sigma(O-\bar{O})^2} \qquad 2)$$

where P is the predicted depth value, O is the observed depth and $\bar{O}$ is the average of the observed depth measurements. The table was exported again into R software for linear regression analysis

4.4 HAB–2 Model

The model originally developed by Fonstad and Marcus (2005) is based on the Beer-Lambert Law that characterizes the exponential absorption of light in water:

$$I = I_0 e^{-\beta D} \qquad 4)$$

where I is the light intensity at a certain depth, I_0 is the light intensity before entering water column, e – the base of natural log, β – diffuse attenuation coefficient constant, and D – depth. Since the information on light intensity is missing in photos, it is being suggested (Fonstad and Marcus, 2005; Walther et al., 2012) to use pixel values from images as they will represent the amount of light reflected into a sensor, thus equation 4 becomes:

$$DN = DN_0 e^{-\beta D} \qquad 5)$$

where DN is the digital number of a pixel and DN_0 – digital number of a pixel immediately adjacent to water. Equation 5 could be rearranged for depth D:

$$D = \frac{LN(\frac{DN}{DN_0})}{-\beta} \qquad 6)$$

The only remaining unknown variable in these equations is the diffuse attenuation coefficient β, which is conventionally being measured with Secchi disk. As rivers are not sufficiently deep for Secchi disk and the historical images lack the field measurements taken at the time of the flight, the value of the diffuse attenuation coefficient had to be estimated (Fonstad and Marcus, 2005; Walther et al., 2012). A seed value of 1.0 for β, as suggested by Fonstad and Marcus (2005) and Walther et al. (2012), was used in equation 6 to estimate the depths along a cross section to calculate the hydraulic radius and the area of a cross-section. This would allow calculating discharge Q ($m^3\ s^{-1}$):

$$Q = AV = WD_aV \qquad 7)$$

where A is the cross-sectional area (m^2), W is the width of the cross section (m), D_a is the average of the predicted depths with the initial seed value (m), and V is the average velocity ($m\ s^{-1}$) calculated with the Manning formula as:

$$V = \frac{R^{2/3} S^{1/2}}{n} \qquad 8)$$

where R is the hydraulic radius (m), S is the longitudinal energy gradient ($m*m^{-1}$) of a flow and n is the Manning hydraulic resistance calculated using Jarrett (1984) equation and shown by Marcus et al. (1992) to be the most suitable for mountainous rivers (Fonstad and Marcus, 2005; Walther et al., 2012):

$$n = 0.32\, S^{0.38} R^{-0.16} \qquad 9)$$

Assuming that hydraulic radius R equals the average depth in a cross section D_a, substitute equations 8 and 9 into equation 7 and solve for discharge Q:

$$Q = \frac{W\, D_a^{1.83}\, S^{0.12}}{0.32} \qquad 10)$$

Since the first estimation of the discharge would not equal the discharge from the gaging station registered for the day of the flight when the imagery was captured, several iterations of seed values of β need to be tried until the calculated discharge equals the recorded one. Once such value is attained, the equation 6 is then applied to the extracted river channel raster.

In this study this equation was applied to the extracted red band, since it has been recommended by other studies (Fonstad and Marcus, 2005; Walther et al., 2012) as the suitable band for the depth prediction. Equation 6 was applied to the extracted red bands for both UAV and the orthorectified Geomont image sets in ArcGIS using <Raster Calculator> tool.

4.5 Band Ratio Model

Since this approach requires taking the natural log of a band ratio, a raster with floating point numbers was created in ArcGIS by using the <Raster Calculator> tool and the equation, followed by the same procedure as discussed in section 4.3:

$$LN(Float\left(\frac{Green\ Band}{Red\ band}\right)) \qquad 11)$$

5. Results

The bathymetry maps produced by the models were compared with the field observations to compute R^2 and Nash-Sutcliffe coefficients (Table 1). For both coefficients, values as close as possible to 1 indicate a very good overall performance of model predictions. The R^2 coefficient shows "how much of the variability in the response variable is explained by the explanatory variable" (Lang and Secic, 2006, p. 91). As for the Nash-Sutcliffe coefficient, if the value is less or equal to 0, than "the model is no better than using the observed mean as predictor" (Gupta et al., 2009). The equations derived from the model calibrations are provided in Table 2.

Table 1: Coefficient values resulting from the linear regression of the predicted and observed depths

Approach	R^2	Nash-Sutcliffe
Red Band Correlation	0.251	0.241
HAB-2	0.329	−0.805
Band Ratio	0.165	0.169

Table 2: The equations derived from the algorithm calibrations

Approach	Model Equation
Red Band Correlation	y = −0.0079x + 1.7118
HAB-2	$\frac{LN(Float(\frac{\text{raster}^1}{233}))}{-1.6228}$
Band Ratio	y = −4.2889x + 0.3621

The bathymetry maps resulting from the correlational model, the HAB-2 model and the band ratio model are presented in Figure 9. The relative maps produced by HAB-2 model applied to two image sets originating from the UAV and Geomont data are illustrated in Figure 10.

[1] Raster – the filenames of the separated red bands from the examined photos.

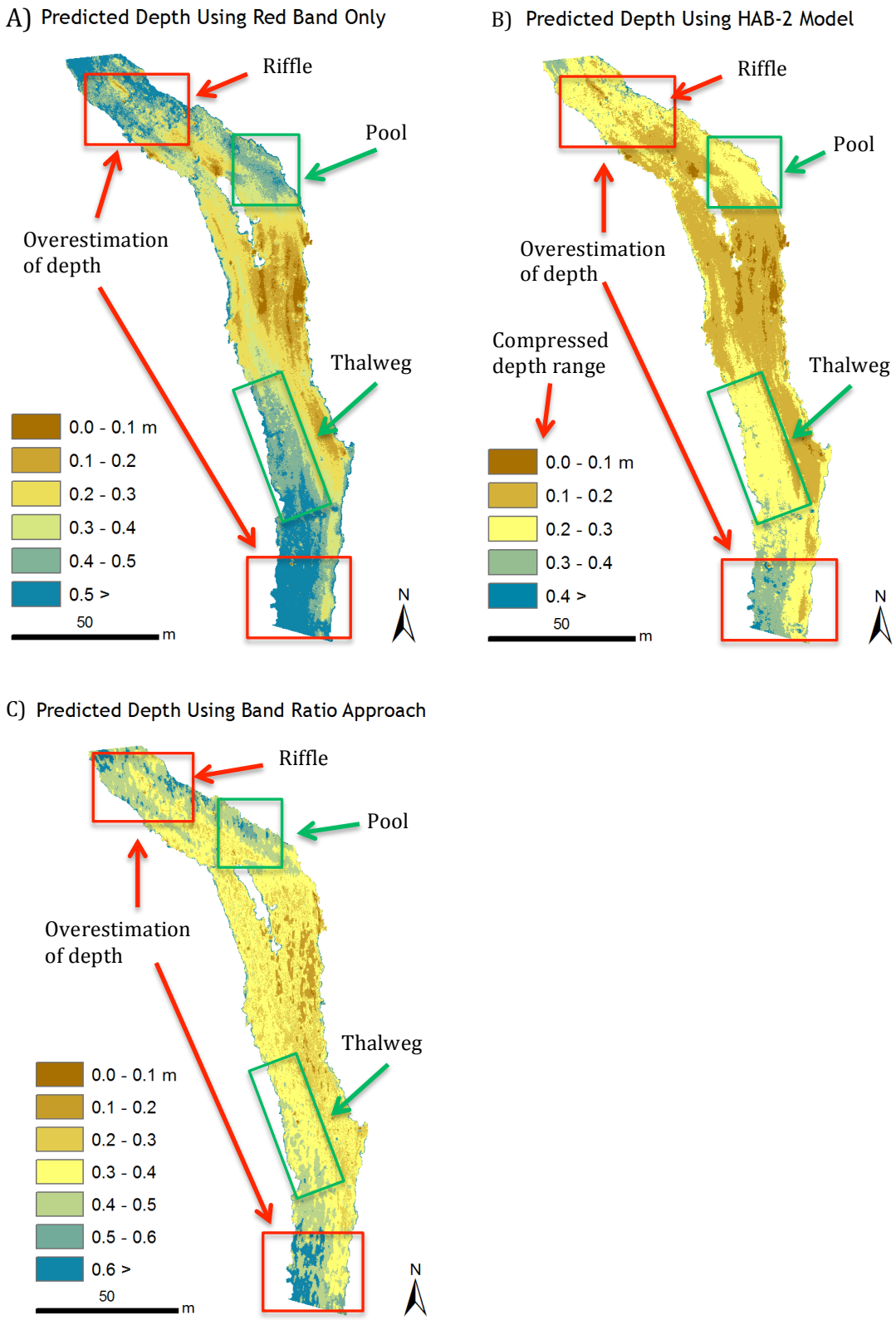

Figure 9: The resulting bathymetry maps produced by the correlation of the red band (A), HAB-2 (B) and the band ratio (C) models.

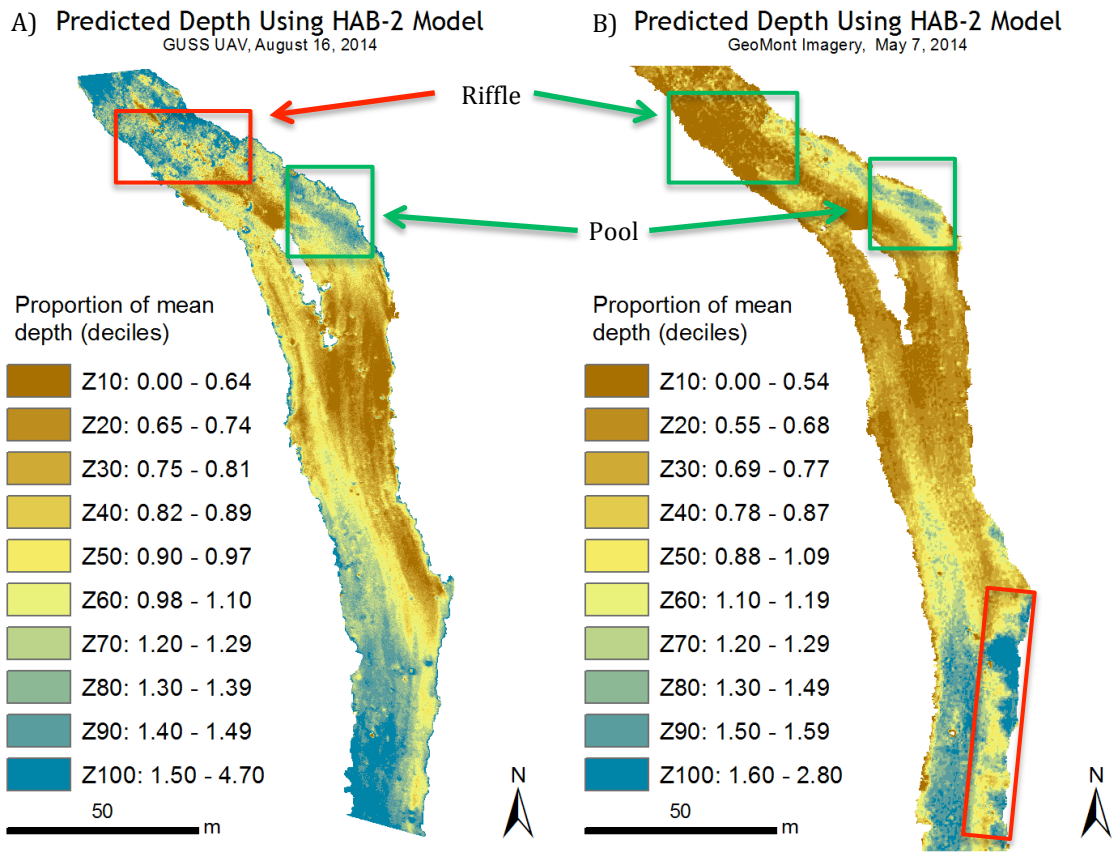

Figure 10: The relative comparison of the bathymetry maps produced by HAB-2 model for the UAV (A) and Geomont data (B).

As shown in Figure 9, all bathymetry maps resulted in correct representation of the pool and part of the thalweg present in the study river. Nonetheless, there are some consistent issues observed on all maps – the overestimation of depth occurring in the riffle zone and part of the thalweg at the edge of the map, which coincide with the edges of the UAV images. There is significant compression of the range of depth predictions on the HAB-2 map (Figure 9b), which is reduced by almost 50% in comparison with the other bathymetry maps. This compression is also confirmed by field observations of the study river reach. Additional problem of depth overestimation along the banks is observed to a certain degree on all maps

although it is mostly visible on the map produced by the correlation of the red band (Figure 9a).

Comparing the HAB-2 approach from the UAV and the Geomont datasets is complicated by the fact that discharge differed between the dates of photo acquisition. To circumvent this problem, the absolute depth estimations were converted into the proportion of the mean depth and represented as deciles. As indicated on Figure 10, the problems of overestimation in the riffle and thalweg zones, and along the banks do not appear on the map produced from Geomont image. The riffle zone is correctly presented as a shallower zone than the nearby pool. The Geomont map predicts the pool and the thalweg in accurate way, although along the right bank (red rectangle, Figure 10b) other pools appeared, which are not found on the maps resulting from the UAV photos.

Figure 11 displays the correlations between the predicted and observed depths throughout the whole study river reach for all models. As it is seen in Figure 11 there is less correlation for the band ratio model than the red band correlational and HAB-2 models, reconfirming the findings summarized in Table 1. The scatter plot for the band ratio (Figure 11c) shows a horizontal trend for some points due to the exactly the same pixel values for the green and red bands.

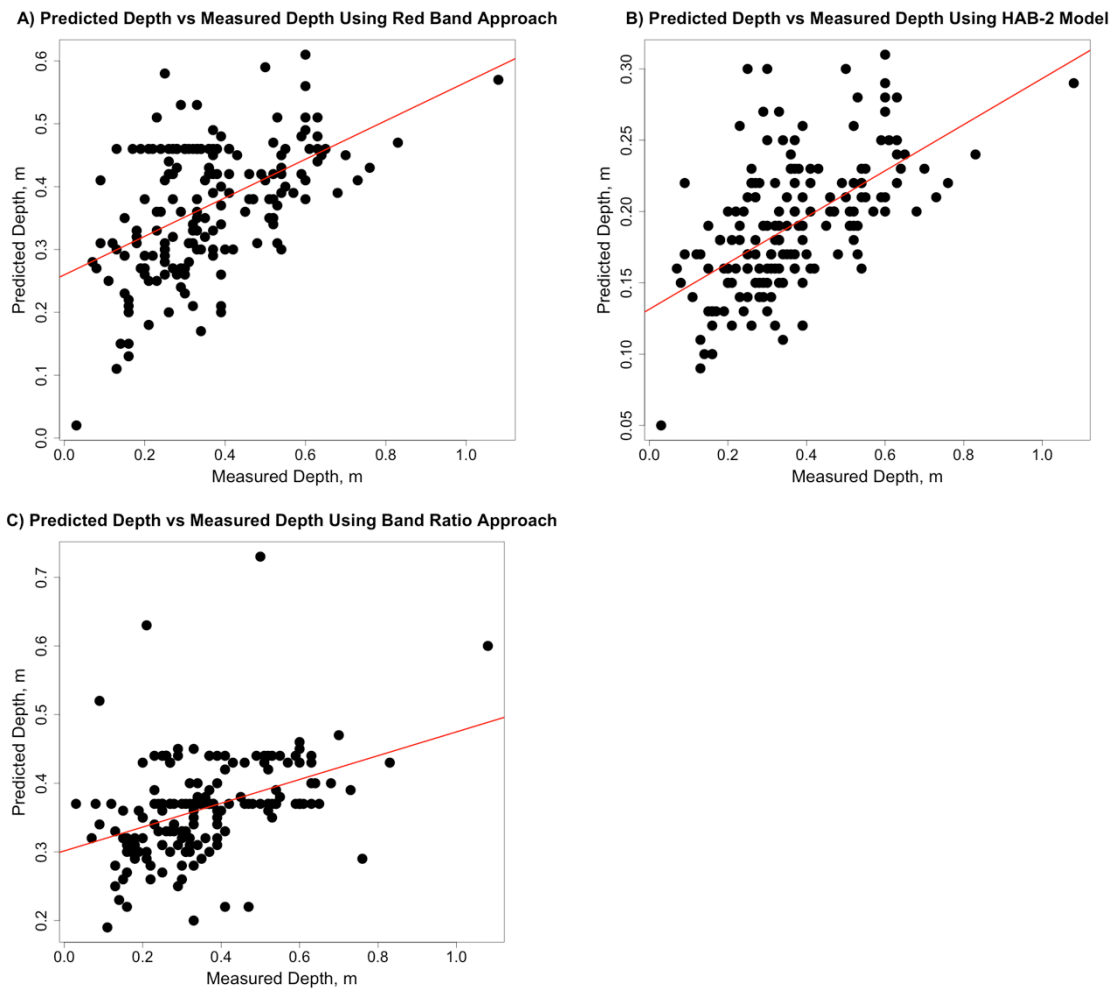

Figure 11: Correlation of predicted and measured depths for the correlational (A), HAB-2 (B) and band ratio (C) models.

Considering that the models might perform differently depending on the habitat type or the relative depth, the separate correlations have been tried for the riffle, pool, shallow and thalweg sections. Table 3 presents the correlation, R^2 and Nash-Sutcliffe Efficiency Model coefficients grouped by the examined approach and selected study zone. These correlations do not include the outliers found in the shadow zones (see Figure 12 for outliers, where green points represent the field measurements). The best correlation is observed in the pool zone for the red band correlational and HAB-2 models, while the shallow zone displays the worst

correlation between the predicted and observed depths in all approaches (Table 3). Considering that pool habitats are often targeted in river restoration studies, it is encouraging that these sections are those with the closest match with field observations. As for the remaining zones, low R^2 values were observed for all algorithms. Out of the approaches the red band correlational and HAB-2 models are similar in their coefficient values per zone, followed by the band ratio, which shows a decrease in the coefficient values for each zone. Considering Nash-Sutcliffe coefficient, the majority of the values are below 0, which signifies that the observed means are better predictors than the examined models.

Table 3: Correlation and NSE coefficients for the predicted and measured depths per zone

Zone	Red Band Correlation			HAB-2			Band Ratio		
	r	R^2	*NSE*	*r*	R^2	*NSE*	*r*	R^2	*NSE*
pool	0.77	0.59	-0.77	0.78	0.61	-5.21	0.66	0.44	-1.39
riffle	0.48	0.23	0.12	0.47	0.22	-1.82	0.33	0.11	0.11
shallow	0.45	0.21	0.07	0.44	0.19	-0.41	0.32	0.11	-1.02
thalweg	0.52	0.27	0.22	0.53	0.29	-1.81	0.69	0.47	0.25

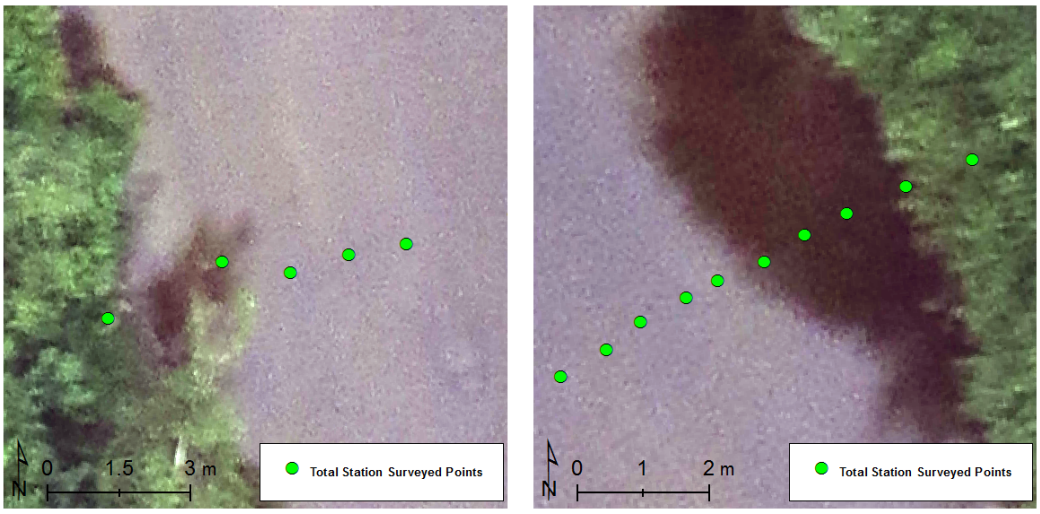

Figure 12: The outliers resulting from shadows

Figure 13 displays the relationship between the predicted and observed depths for separate zones within the reach. There is observable offsetting of the thalweg regression line in both the correlational and HAB-2 models compared to the remaining zones, which follow a similar trend. In the band ratio correlation graph (Figure 13c) the pool section is offset compared to the remaining zones, although the riffle zone shows the lowest correlation of the four regression lines.

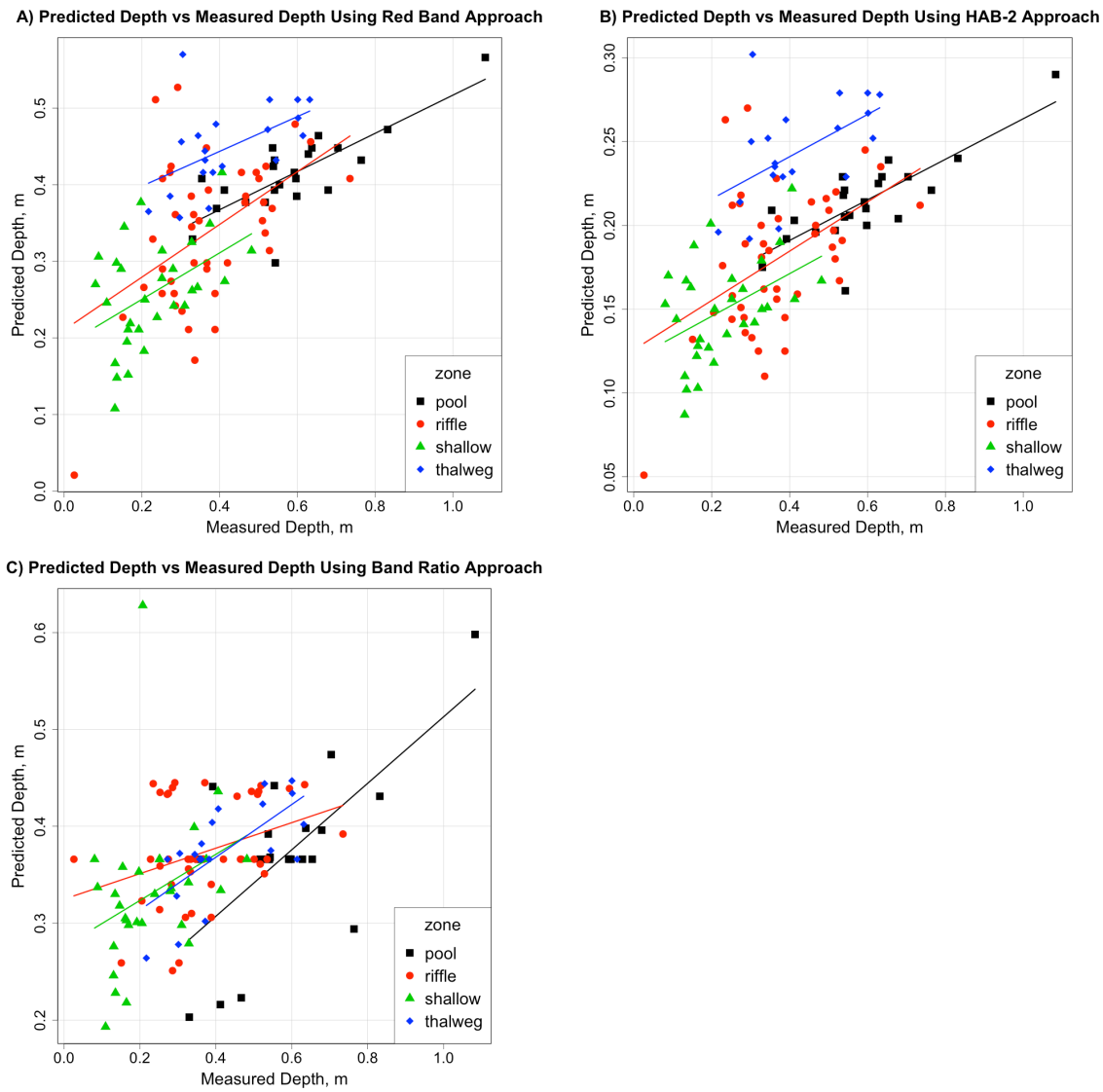

Figure 13: Correlation of predicted and measured depths per zone for the correlational (A), HAB-2 (B) and band ratio (C) models.

6. Discussion

The accuracy of depth predictions and model performance were assessed based on two coefficients, discussed in detail in sections 4.3 and 5. It has been decided not to omit outliers in the model calibrations to provide an unbiased approach to model testing and further data analysis in model validations. However, outliers were removed to compare the quality of the models for specific river sections. Overall, no model performed sufficiently well to be considered for practical use, although there was a better match between predicted models and field measurements when assessing specifically pool areas. Although the coefficient values are substantially far from a perfect fit between the prediction and the observation ($R^2 << 1$ or NSE << 1), they still allow a relative comparison between the models. Somehow R^2 values contradict NSE values in regards to HAB-2 performance – the highest positive R^2 value and the only negative NSE value. As for the other two models (the correlation of the red band and the band ratio), all coefficient values per model are nearly identical and differ by less than 5% in both cases. According to these observations it was expected that NSE value for HAB-2 model would follow a similar trend. The correlation of the red band with the field measurements offered the best accuracy, followed by the band ratio model predictions (Table 1). The negative NSE value for HAB-2 model leads to uncertainty as to how the model truly performed despite having the largest R^2 value.

The increased correlation and R^2 coefficients for the pool zone (Table 3 and Figure 13) is nevertheless encouraging since mapping pool zones is often an objective in river studies, for example to assess the quality of fish habitat

(Montgomery and Buffington, 1993; Wited et al., 2002; Bisson et al., 2011). If, however, a study aims at quantifying riffle areas, the use of true-colour photographs is not recommended based on the findings of this study. The better correlation in the pool area can be partly explained by the fact that outliers due to shadow zones were removed for this analysis

The produced maps reveal some issues related to the quality of the aerial photos captured with the camera installed in the UAV. Figures 9 displays several common problems originating from the source images. Due to the presence of vignette on the original photos, depth overestimation in the riffle and part of the thalweg areas occurred on all three bathymetry maps. These areas coincide with the edges of the UAV images, where the vignette usually occurs because of lower-grade lens. From the personal knowledge of the study reach and observations of the riffle area, it can be confirmed that the depths did not exceed 20 cm. Similar observations can be made in the thalweg area, where the recorded depths were below 40 cm (see Figure 9). The other places where overestimation has occurred are along the banks. In this case it was caused by the presence of shadow from slightly steep banks or vegetation such as small trees or bushes. On the other hand, all the maps correctly predicted the position of the pool in proximity to the bar, situated in the middle of the river reach, and part of the thalweg, as well as the large shallow area between the thalweg and the bar.

Most of the aforementioned problems with depth overestimation are not observed on the bathymetry map produced by HAB-2 model, which was applied to Geomont image (Figure 10b). Both the riffle and the thalweg areas were relatively

correctly represented in terms of estimated depths. Due to different weather conditions, the banks did not create shadows. However, the presence of larger trees on the right bank created a series of unnaturally looking pools along the right edge of the river channel (see Figure 10 and 14), which highlight the challenge related to bank vegetation described by several researchers (Roberts and Anderson, 1999; Feurer et al., 2008; Flener et al., 2012). Better characterization of the river topography by HAB-2 model on the Geomont image suggests the potential preference of this dataset over the UAV platform for further testing of the algorithms.

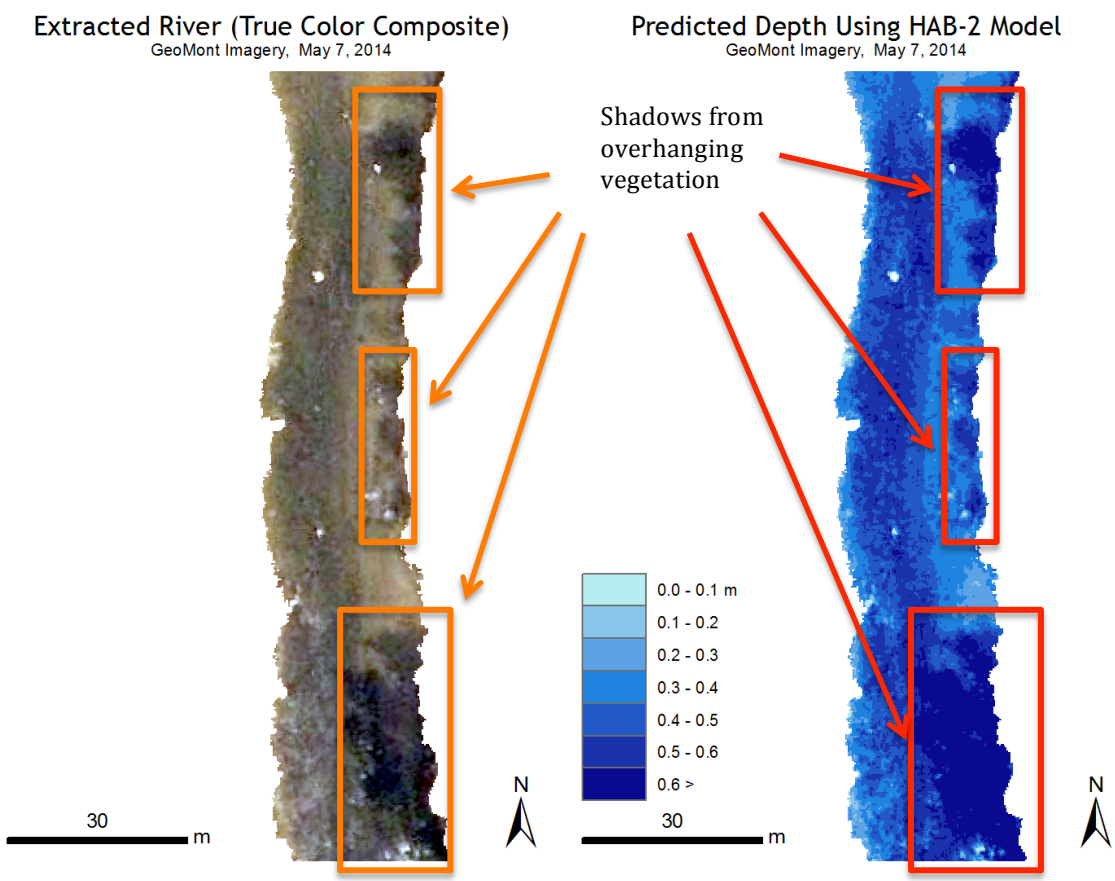

Figure 14: The depth overestimation resulting from the presence of shadows

HAB-2 bathymetry map offered smaller depth range in the study reach in comparison to the other algorithms with a possible explanation of using incorrectly assumed value(s) in the model calibration (Figure 9b). Considering that the same methodology was applied to the Geomont image, similar smaller values of predicted depths could have been detected. Due to the absence of field measurements of the same river reach for the date when the flight took place, it is impossible to confirm this assumption.

The accuracy of georeferencing could be mentioned as one of potential reasons for poor performance of all models. Both the UAV images and the topography points required to be correctly positioned in relation to each other as well as to an absolute datum, thus adding up the positioning errors. This could have been resolved by using other technologies such as digital global positioning system (DGPS) surveying tool, which are becoming increasingly affordable. In addition to this, the geometric distortion by the camera lens has contributed to the issue of georeferencing of the datasets. The correct position of the topography depth measurements overlaid on top of the UAV imagery is important. The captured imagery has ~4 cm/pixel spatial resolution and might be too sensitive to depth variation as it has been described by Walther et al. (2012). The topography points might not overlay perfectly the correct pixels representing exactly the same locations in the river. Carbonneau and Piégay (2012) mention as well the scale distortions in the optical imagery, poor selection of ground control points for georeferencing and the algorithms used for the image transformation to a specific coordinate system as potential sources for error generation.

One issue applicable only to the band ratio model is the extraction of the same pixel values from both bands. Since the algorithm uses the natural log of the band ratio to provide linearity in the model calibration with the observed measurements, the resulting zeroes – for instance, LN(96/96) = 0 versus LN(119/119) = 0 – are seen by the model as the same depth, thus altering the equation for the best-fit line (see Figure 11c for the observed horizontal trend due to the same pixel values in both bands after the model calibration). Considering the original pixel values, which differ substantially in the given example, the suggestion of Legleiter and Roberts (2005) to select the green and red bands might not be appropriate and other band ratios should be tested.

Finally, models were examined under specific weather conditions with a heavily overcast sky at the time of the UAV flight. This contributed to the creation of smaller aforementioned noticeable shadows along the banks, which led to the overestimation of the depth in these areas. It would have been interesting to be able to compare the situation with UAV images taken under sunny conditions, although time of the day still remains one of the considerations to avoid the appearance of shadows.

7. Conclusion

Neither of the tested models performed well enough to be considered for practical use and provide trustworthy absolute quantifiable estimations of depth in the study river reach, although pools were better predicted than other features such as riffles.

Nonetheless, some of the algorithms such as the correlational or HAB-2 models still could be used either for relative comparison of the same study reach over the temporal scale, which would allow to observe any happening trends in riverbed development due to erosion or deposition, or to qualitatively characterize rivers. At the same time, provided that the bathymetry maps are correctly georeferenced to an absolute datum, the relative position of morphological units such as pools, riffles or other in-stream features could be derived. Although the depth predicted by the models will not be reliable, the width and length of in-stream habitats could be of potential usefulness to some researches. Judging by some of the study zones, particularly deeper areas such as the pool and thalweg zones, actually displayed an improvement in correlation between the predicted and observed depths in the pool and thalweg zones (Table 3).

One possible improvement in this experiment would have been the replacement of the digital camera carried by the UAV to rectify the problems of vignette and geometric distortion. A camera such as DSLR with more expensive high-quality lens could eliminate vignetting and distortion or bring it to a negligible minimum. The removal of vignette observed on the UAV imagery would otherwise correct the problem of overestimation of depth along the photo edges. The higher-

grade lens would suggest the correction of potential geometric distortion, which would contribute to better georeferencing accuracy. Although the recommendation would require certain budget increase, the platform of choice in this study will nevertheless remain in the least expensive sector of the available commercial UAV solutions, some of which are bundled with more sophisticated equipment and software.

The quality of aerial images is another aspect of important consideration in remote depth mapping. Out of two aerial datasets obtained in this study, the orthorectified imagery distributed by Geomont has shown promising potential results in HAB-2 model testing. Since the imagery comes already corrected for the geometric distortion and has not displayed the other problems, which were characteristic to the UAV dataset, such as no overestimation of depth in the riffle and part of thalweg zones, and along the banks, further usefulness of these images for depth prediction could be examined.

Although the main objective of the study is the assessment of the applicability of true-colour imagery, consisting only of red, green and blue bands, it is should be mentioned that there are other type of sensors, which could be certainly used for depth estimation. Certain models of digital cameras could be modified to fit infrared filter to provide the fourth band, which could be usefully applied to the band ratio approach. It has been recommended by Legleiter and Roberts (2005) that the numerator band in a ratio should be least sensitive, while the band in the denominator to be the most sensitive to light absorption by water. The infrared band has proven to be the most suitable band to be used in a band ratio (Legleiter

and Roberts, 2005), since the infrared part of the spectrum of the light energy is the quickest to be absorbed by water column.

The results obtained in this study demonstrate that in the context of the Yamaska Sud-Est River, the methodology and the experiment design, neither of the established research questions has been positively answered. The produced bathymetry maps provided some unreliable depth estimations for the study river reach, revealing that the true-colour images obtained from the digital camera GUSS UAV and the examined models have minimal applicability under these conditions. At the same time due to the complexity of the experiment and methodology with many considerations regarding variables and the equipment, it still remains unclear if the difference in the testing and original environments caused any issue in the model performances. The algorithms remain to be tested further for proper evaluation of their applicability outside the original environment where they were developed. It would be possible to truly estimate their performance once the other aforementioned issues have been taken into account.

References:

3DR uBlox GPS with Compass Kit - 3DRobotics Inc. (n.d.). Retrieved 11 April 2015, from http://store.3drobotics.com/products/3dr-gps-ublox-with-compass

APM 2.6 Set - 3DRobotics Inc. (n.d.). Retrieved 11 April 2015, from http://store.3drobotics.com/products/apm-2-6-kit-1

Bird, S., Hogan, D., & Schwab, J. (2010). Photogrammetric monitoring of small streams under a riparian forest canopy. *Earth Surface Processes and Landforms*, *35*(8), 952-970.

Bisson, P., Montgomery, D., Buffington, J. *Valley segments, stream reaches, and channel units.* In *Methods in stream ecology*. Hauer, F. R., & Lamberti, G. A. (Eds.). (2011). Academic Press.

Carbonneau, P., Fonstad, M. A., Marcus, W. A., & Dugdale, S. J. (2012). Making riverscapes real. *Geomorphology, 137*(1), 74-86. doi:10.1016/j.geomorph.2010.09.030

Carbonneau, P., Lane, S., & Bergeron, N. (2004). Catchment-scale mapping of surface grain size in gravel bed rivers using airborne digital imagery. *Water Resources Research*, 40(7), W07202. doi:10.1029/2003WR002759

Carbonneau, P. E., Lane, S. N., & Bergeron, N. (2006). Feature based image processing methods applied to bathymetric measurements from airborne remote sensing in fluvial environments. *Earth Surface Processes and Landforms, 31*(11), 1413-1423. doi:10.1002/esp.1341

Carbonneau, P., & Piégay, H. (2012). Fluvial remote sensing for science and management. Chichester, West Sussex, UK: Wiley-Blackwell.

Choné, G. (2013). *L'espace de mobilité des rivières du sud du Québec : implications pour les écosystèmes et la gestion des rivières dans une perspective de changements climatiques.* Unpublished masters thesis, Concordia University, Québec.

Dunford, R., Michel, K., Gagnage, M., Piegay, H., & Tremelo, M. -L. (2009). Potential and constraints of unmanned aerial vehicle technology for the characterization of mediterranean riparian forest. *International Journal of Remote Sensing, 30*(19), 4915-4935. doi:10.1080/01431160903023025

Fausch, K. D., Torgersen, C. E., Baxter, C. V., & Li, H. W. (2002). Landscapes to riverscapes: bridging the gap between research and conservation of stream fishes a continuous view of the river is needed to understand how processes

interacting among scales set the context for stream fishes and their habitat. *BioScience*, *52*(6), 483-498.

Feurer, D., Bailly, J., Puech, C., Le Coarer, Y., & Viau, A. A. (2008). Very-high-resolution mapping of river-immersed topography by remote sensing. *Progress in Physical Geography, 32*(4), 403-419. doi:10.1177/0309133308096030

Flener, C. (2013). Estimating deep water radiance in shallow water: Adapting optical bathymetry modelling to shallow river environments. *Boreal Environment Research, 18*(6), 488-502.

Flener, C., Lotsari, E., Alho, P., & Kayhko, J. (2012). Comparison of empirical and theoretical remote sensing based bathymetry models in river environments. *River Research and Applications, 28*(1), 118-133. doi:10.1002/rra.1441

Flener, C., Vaaja, M., Jaakkola, A., Krooks, A., Kaartinen, H., Kukko, A., . . . Alho, P. (2013). Seamless mapping of river channels at high resolution using mobile LiDAR and UAV-photography. *Remote Sensing, 5*(12), 6382-6407. doi:10.3390/rs5126382

Fonstad, M., & Marcus, W. (2005). Remote sensing of stream depths with hydraulically assisted bathymetry (HAB) models. *Geomorphology, 72*(1-4), 320-339. doi:10.1016/j.geomorph.2005.06.005

Fonstad, M. A., & Marcus, W. A. (2010). High resolution, basin extent observations and implications for understanding river form and process. *Earth Surface Processes and Landforms, 35*(6), 680-698. doi:10.1002/esp.1969

Gilvear, D., & Bryant, R. (2003). Analysis of aerial photography and other remotely sensed data. Red, 600(5.8), 23.

Gilvear, D., Hunter, P., & Higgins, T. (2007). An experimental approach to the measurement of the effects of water depth and substrate on optical and near infra-red reflectance: A field-based assessment of the feasibility of mapping submerged instream habitat. *International Journal of Remote Sensing, 28*(10), 2241-2256. doi:10.1080/01431160600976079

Gupta, H. V., Kling, H., Yilmaz, K. K., & Martinez, G. F. (2009). Decomposition of the mean squared error and NSE performance criteria: Implications for improving hydrological modelling. Journal of Hydrology, 377(1), 80-91.

Hilldale, R. C., & Raff, D. (2008). Assessing the ability of airborne LiDAR to map river bathymetry. *Earth Surface Processes and Landforms, 33*(5), 773-783. doi:10.1002/esp.1575

Kinzel, P. J., Legleiter, C. J., & Nelson, J. M. (2012). Mapping river bathymetry with a small footprint green LiDAR: Applications and challenges. *Journal of the American Water Resources Association, 49*(1), 183-204. doi:10.1111/jawr.12008

Jarrett, R. D. (1984). Hydraulics of high-gradient streams. *Journal of Hydraulic Engineering*, *110*(11), 1519-1539.

Lane, S., Hardy, R., Elliott, L., & Ingham, D. (2002). High-resolution numerical modelling of three-dimensional flows over complex river bed topography. *Hydrological Processes, 16*(11), 2261-2272. doi:10.1002/hyp.5034

Lane, S., & Chandler, J. (2003). Editorial: The generation of high quality topographic data for hydrology and geomorphology: New data sources, new applications and new problems. Earth Surface Processes and Landforms, 28(3), 229-230. doi:10.1002/esp.479

Lane, S. N., Widdison, P. E., Thomas, R. E., Ashworth, P. J., Best, J. L., Lunt, I. A., . . . Simpson, C. J. (2010). Quantification of braided river channel change using archival digital image analysis. *Earth Surface Processes and Landforms, 35*(8), 971-985. doi:10.1002/esp.2015

Lang, T. A., & Secic, M. (2006). *How to report statistics in medicine: annotated guidelines for authors, editors, and reviewers*. ACP Press.

Legleiter, C. (2003). Spectrally driven classification of high spatial resolution, hyperspectral imagery: A tool for mapping in-stream habitat. *Environmental Management, 32*(3), 399-411. doi:10.1007/s00267-003-0034-1

Legleiter, C. J. (2012). Remote measurement of river morphology via fusion of LiDAR topography and spectrally based bathymetry. *Earth Surface Processes and Landforms, 37*(5), 499-518. doi:10.1002/esp.2262

Legleiter, C. J. (2013). Mapping river depth from publicly available aerial images. *River Research and Applications, 29*(6), 760-780. doi:10.1002/rra.2560

Legleiter, C. J., & Overstreet, B. T. (2012). Mapping gravel bed river bathymetry from space. *Journal of Geophysical Research-Earth Surface, 117*, F04024. doi:10.1029/2012JF002539

Legleiter, C., & Roberts, D. (2005). Effects of channel morphology and sensor spatial resolution on image-derived depth estimates. *Remote Sensing of Environment, 95*(2), 231-247. doi:10.1016/j.rse.2004.12.013

Legleiter, C. J., & Roberts, D. A. (2009). A forward image model for passive optical remote sensing of river bathymetry. *Remote Sensing of Environment, 113*(5), 1025-1045. doi:10.1016/j.rse.2009.01.018

Legleiter, C., Roberts, D., Marcus, W., & Fonstad, M. (2004). Passive optical remote sensing of river channel morphology and in-stream habitat: Physical basis and feasibility. *Remote Sensing of Environment, 93*(4), 493-510. doi:10.1016/j.rse.2004.07.019

Legleiter, C. J., Roberts, D. A., & Lawrence, R. L. (2009). Spectrally based remote sensing of river bathymetry. *Earth Surface Processes and Landforms, 34*(8), 1039-1059. doi:10.1002/esp.1787

Lyzenga, D. R. (1981). Remote sensing of bottom reflectance and water attenuation parameters in shallow water using aircraft and Landsat data. *International Journal of Remote Sensing*, *2*(1), 71-82.

Marcus, W. A., Roberts, K., Harvey, L., & Tackman, G. (1992). An evaluation of methods for estimating Manning's n in small mountain streams. *Mountain Research and Development*, 227-239.

Marcus, W. A., & Fonstad, M. A. (2008). Optical remote mapping of rivers at sub-meter resolutions and watershed extents. *Earth Surface Processes and Landforms, 33*(1), 4-24. doi:10.1002/esp.1637

Marcus, W. A., & Fonstad, M. A. (2010). Remote sensing of rivers: The emergence of a subdiscipline in the river sciences. *Earth Surface Processes and Landforms, 35*(15), 1867-1872. doi:10.1002/esp.2094

Marcus, W., Legleiter, C., Aspinall, R., Boardman, J., & Crabtree, R. (2003). High spatial resolution hyperspectral mapping of in-stream habitats, depths, and woody debris in mountain streams. *Geomorphology, 55*(1-4), 363-380. doi:10.1016/S0169-555X(03)00150-8

McKenzie, N., & Ryan, P. (1999). Spatial prediction of soil properties using environmental correlation. *Geoderma, 89*(1-2), 67-94. doi:10.1016/S0016-7061(98)00137-2

Metternicht, G., Hurni, L., & Gogu, R. (2005). Remote sensing of landslides: An analysis of the potential contribution to geo-spatial systems for hazard assessment in mountainous environments. *Remote Sensing of Environment*, 98(2-3), 284-303. doi:10.1016/j.rse.2005.08.004

Mission Planner | Ground Station. (n.d.). Retrieved 11 April 2015, from http://planner.ardupilot.com/

Montgomery, D. R., & Buffington, J. M. (1993). *Channel classification, prediction of channel response, and assessment of channel condition* (p. 107). Washington State Timber, Fish & Wildlife.

Moretto, J., Rigon, E., Mao, L., Delai, F., Picco, L., & Lenzi, M. A. (2014). Short-term geomorphic analysis in a disturbed fluvial environment by fusion of LiDAR, colour bathymetry and dGPS surveys. *Catena, 122*, 180-195. doi:10.1016/j.catena.2014.06.023

Roberts, A., & Anderson, J. (1999). Shallow water bathymetry using integrated airborne multi-spectral remote sensing. *International Journal of Remote Sensing, 20*(3), 497-510. doi:10.1080/014311699213299

Visser, F., Wallis, C., & Sinnott, A. M. (2013). Optical remote sensing of submerged aquatic vegetation: Opportunities for shallow clearwater streams. *Limnologica, 43*(5), 388-398. doi:10.1016/j.limno.2013.05.005

Waddle, T., Steffler, P., Ghanem, A., Katopodis, C., & Locke, A. (2000). Comparison of one and two-dimensional open channel flow models for a small habitat stream. *Rivers, 7*(3), 205-220.

Walther, S. C., Marcus, W. A., & Fonstad, M. A. (2011). Evaluation of high-resolution, true-colour, aerial imagery for mapping bathymetry in a clear-water river without ground-based depth measurements. *International Journal of Remote Sensing, 32*(15), 4343-4363. doi:10.1080/01431161.2010.486418

Westaway, R., Lane, S., & Hicks, D. (2001). Remote sensing of clear-water, shallow, gravel-bed rivers using digital photogrammetry. *Photogrammetric Engineering and Remote Sensing, 67*(11), 1271-1281.

Whited, D., Stanford, J., & Kimball, J. (2002). Application of airborne multispectral digital imagery to quantify riverine habitats at different base flows. *River Research and Applications, 18*(6), 583-594. doi:10.1002/rra.695

Whited, D. C., Kimball, J. S., Lorang, M. S., & Stanford, J. A. (2013). Estimation of juvenile salmon habitat in pacific rim rivers using multiscalar remote sensing and geospatial analysis. *River Research and Applications, 29*(2), 135-148. doi:10.1002/rra.1585

Winterbottom, S., & Gilvear, D. (1997). Quantification of channel bed morphology in gravel-bed rivers using airborne multispectral imagery and aerial photography. *Regulated Rivers-Research & Management, 13*(6), 489-499. doi:10.1002/(SICI)1099-1646(199711/12)13:6<489::AID-RRR471>3.0.CO;2-X

Wirth, L., Rosenberger, A., Prakash, A., Gens, R., Margraf, F. J., & Hamazaki, T. (2012). A remote-sensing, GIS-based approach to identify, characterize, and model spawning habitat for fall-run chum salmon in a sub-arctic, glacially fed river. *Transactions of the American Fisheries Society, 141*(5), 1349-1363. doi:10.1080/00028487.2012.692348